Selective targeting of engineered T cells using orthogonal IL-2 cytokine-receptor complexes

Jonathan T. Sockolosky[1,2], **Eleonora Trotta**[3,*], **Giulia Parisi**[4,*], **Lora Picton**[1], **Leon L. Su**[1], **Alan C. Le**[5], **Akanksha Chhabra**[5], **Stephanie L. Silveria**[3], **Benson M. George**[2,5,6], **Indigo C. King**[7], **Matthew R. Tiffany**[8], **Kevin Jude**[1], **Leah V. Sibener**[1,9], **David Baker**[7], **Judith A. Shizuru**[5], **Antoni Ribas**[4,10], **Jeffrey A. Bluestone**[3,10], and **K. Christopher Garcia**[1,2,10,11,†]

[1]Departments of Molecular and Cellular Physiology and Structural Biology, Stanford University School of Medicine, Stanford, CA 94305, USA

[2]Stanford Cancer Institute, Stanford University School of Medicine, Stanford, CA 94305, USA

[3]Diabetes Center and Department of Medicine, University of California, San Francisco, CA 94143, USA

[4]Division of Hematology-Oncology, Department of Medicine, David Geffen School of Medicine, and Jonsson Comprehensive Cancer Center, University of California, Los Angeles, CA 90095, USA

[5]Department of Blood and Marrow Transplantation, Institute for Stem Cell Biology and Regenerative Medicine, and Ludwig Center for Cancer Stem Cell Research and Medicine, Stanford University School of Medicine, Stanford, CA 94305, USA

[6]Stanford Medical Scientist Training Program, Stanford University, Stanford, CA 94305, USA

[7]Department of Biochemistry, Howard Hughes Medical Institute, and Institute for Protein Design, University of Washington, Seattle, WA 98195, USA

[8]Department of Pediatrics and Genetics, Stanford University School of Medicine, Stanford, CA 94305, USA

[9]Immunology Graduate Program, Stanford University School of Medicine, Stanford, CA 94305, USA

[10]Parker Institute for Cancer Immunotherapy, 1 Letterman Drive, Suite D3500, San Francisco, CA 94129, USA

[11]Howard Hughes Medical Institute, Stanford University School of Medicine, Stanford, CA 94305, USA

[†]Corresponding author. Email: kcgarcia@stanford.edu.
[*]These authors contributed equally to this work.

SUPPLEMENTARY MATERIALS

www.sciencemag.org/content/359/6379/1037/suppl/DC1

Materials and Methods

Figs. S1 to S18

References (29–35)

Abstract

Interleukin-2 (IL-2) is a cytokine required for effector T cell expansion, survival, and function, especially for engineered T cells in adoptive cell immunotherapy, but its pleiotropy leads to simultaneous stimulation and suppression of immune responses as well as systemic toxicity, limiting its therapeutic use. We engineered IL-2 cytokine-receptor orthogonal (*ortho*) pairs that interact with one another, transmitting native IL-2 signals, but do not interact with their natural cytokine and receptor counterparts. Introduction of *ortho*IL-2Rβ into T cells enabled the selective cellular targeting of *ortho*IL-2 to engineered CD4$^+$ and CD8$^+$ T cells in vitro and in vivo, with limited off-target effects and negligible toxicity. *Ortho*IL-2 pairs were efficacious in a preclinical mouse cancer model of adoptive cell therapy and may therefore represent a synthetic approach to achieving selective potentiation of engineered cells.

Adoptive transfer of tumor-reactive T cells has evolved into a clinically useful therapy capable of inducing antitumor immunity in patients (1, 2). However, the broad application of adoptive T cell transfer (ACT) therapies to treat cancer has several limitations, including the production of sufficient quantities of cells for infusion and the failure of transferred T cells to persist and remain functional in vivo. In the clinic, the concomitant administration of the T cell growth factor interleukin-2 (IL-2) improves the survival, function, and antitumor activity of transplanted T cells (3, 4). However, the use of IL-2 to potentiate ACT is complicated by the pleiotropic nature of IL-2, which induces both immune stimulatory and suppressive T cell responses as well as potentially severe toxicities (5). This is governed by the interaction between IL-2 and the IL-2 receptor (IL-2R), which consists of α, β, and γ subunits (6). IL-2Rβ and the common γ-chain (IL-2Rγ) together form the signaling dimer and bind IL-2 with moderate affinity, whereas IL-2Rα (CD25) does not signal but increases the affinity of IL-2 for the binary (βγ) IL-2 receptor to sensitize T cells to low concentrations of IL-2.

The activity of IL-2 as an adjuvant to ACT is dependent on the balance between activation of transplanted and endogenous T cell subsets bearing natural IL-2 receptors, as well as host responses that cause dose-limiting toxicities. Strategies to overcome these limitations could improve T cell immunotherapy (7, 8). Recognizing the need for new approaches that afford precise targeting of IL-2–dependent functions to a specific cell type of interest, we devised a strategy to redirect the specificity of IL-2 toward adoptively transferred T cells. This method, based on receptor-ligand orthogonalization, uses a mutant IL-2 cytokine and mutant IL-2 receptor that bind specifically to one another but not to their wild-type counterparts (Fig. 1A).

We focused on the murine IL-2/IL-2Rβ interaction to enable in vivo characterization in syngeneic mouse models. The IL-2Rβ chain was chosen as the mutant receptor because the β chain is required for signal transduction and can bind IL-2 independently. We devised a two-step approach to engineer orthogonal IL-2/IL-2Rβ pairs informed by the crystal structure of the IL-2 high-affinity receptor complex (6) (Fig. 1B). First, point mutations of the IL-2Rβ chain were identified from inspection of the interface between IL-2 and IL-2Rβ that abrogated binding to wild-type IL-2 (Fig. 1, C to E). The IL-2Rβ hot-spot residues His^{134} and Tyr^{135} make numerous contacts with IL-2 that contribute a majority of the

binding free energy between IL-2 and IL-2Rβ (6) (Fig. 1E). A double mutant IL-2Rβ [His^{134} → Asp (H134D) and Tyr^{135} → Phe (Y135F)], referred to herein as *ortho*IL-2Rβ, lacked detectable binding to IL-2 (Fig. 1D), even in the presence of CD25 (fig. S1) (7, 9).

Next, we used yeast display-based evolution to mutate, and thus remodel, the wild-type IL-2 interface region that was opposing (or facing the site of) the IL-2Rβ mutations in the crystal structure, in order to create a molecule that bound to *ortho*IL-2Rβ but not to wild-type IL-2Rβ. IL-2 residues in proximity to the *ortho*IL-2Rβ binding interface were randomly mutated and were chosen on the basis of a homology model of the mouse IL-2/IL-2Rβ complex (Fig. 1E) derived from the crystal structure of the human IL-2 receptor complex (6). A library of ~10^8 unique IL-2 mutants was displayed on the surface of yeast (fig. S2) and subjected to multiple rounds of both positive (against *ortho*IL-2Rβ) and negative (against IL-2Rβ) selection (figs. S2 and S3). This collection of yeast-displayed IL-2 mutants bound the *ortho*IL-2Rβ, but not wild-type IL-2Rβ, and retained CD25 binding (Fig. 1D). Sequencing of yeast clones from the evolved IL-2 libraries revealed a consensus set of mutations at IL-2 positions in close structural proximity to the *ortho*IL-2Rβ mutations (fig. S4). Interestingly, a Gln^{30} → Asn (Q30N) mutation was highly conserved across three independent mutant IL-2 yeast libraries, whereas all other IL-2 positions used a restricted but not specific mutational signature. We found that IL-2 mutations Q30N, Met^{33} → Val (M33V), and Asp^{34} → Leu or Met (D34L/M) appear to form a small nonpolar pocket to compensate for the IL-2Rβ Y135F mutation, whereas Gln^{36} → Thr, Ser, Lys, or Glu (Q36T/S/K/E) and Glu^{37} → Tyr or His (E37Y/H) mutations present a polar or charged surface to compensate for the IL-2Rβ H134D mutation (Fig. 1F).

Because of the affinity-enhancing effects of CD25 expression on the interaction of IL-2 with the binary (βγ) IL-2 receptor (10), IL-2 mutants with negligible binding to IL-2Rβ alone may still form a functional signaling complex on cells that also express CD25 (8). Therefore, we used a yeast-based functional screen to further triage IL-2 mutants that bound specifically to the *ortho*IL-2Rβ and signaled selectively on T cells that express the *ortho*IL-2Rβ (Fig. 1G and fig. S5), and produced recombinant forms of select IL-2 mutants (*ortho*IL-2) for characterization (figs. S6 to S8).

We focused our efforts on two *ortho*IL-2 mutants, 1G12 and 3A10. *Ortho*IL-2 1G12 and 3A10 share the consensus Q30N, M33V, and D34L mutations but differ at positions Glu^{29}, Gln^{36}, Glu^{37}, and Arg^{41} (Fig. 1I). *Ortho*IL-2 1G12 and 3A10 bound the *ortho*IL-2Rβ with an affinity comparable to that of the wild-type IL-2/IL-2Rβ interaction and displayed little to no detectable binding to wild-type IL-2Rβ (Fig. 1H and figs. S7 and S8) but differed in their ability to activate IL-2Rβ signaling in CD25-positive wild-type and *ortho*IL-2Rβ T cells. Stimulation of *ortho*IL-2Rβ T cells (fig. S5B) with *ortho*IL-2 1G12 resulted in dose-dependent phosphorylation of STAT5 (pSTAT5), a hallmark of IL-2R signaling, with potency similar to that of wild-type IL-2, but also induced pSTAT5 on wild-type T cells, albeit with significantly reduced potency relative to IL-2 (Fig. 1, G and I, and fig. S6). By comparison, *ortho*IL-2 3A10 was specific for *ortho*IL-2Rβ T cells, but with a weaker potency relative to IL-2 (Fig. 1, G and I, and fig. S6). We speculated that *ortho*IL-2 1G12 activity on wild-type T cells is a consequence of weak residual binding to wild-type IL-2Rβ (fig. S7). Low-affinity interactions with IL-2Rβ alone are enhanced in the presence of CD25

(8). Indeed, *ortho*IL-2 1G12 exhibited binding to wild-type IL-2Rβ when first captured by CD25, with limited binding in the absence of CD25 (figs. S1 and S8). *Ortho*IL-2 3A10 did not bind appreciably to IL-2Rβ even in the presence of CD25, in agreement with its negligible biological activity on CD25-positive T cells. Interaction of *ortho*IL-2 1G12 and 3A10 with *ortho*IL-2Rβ was significantly enhanced in the presence of CD25, with apparent binding affinities of the ternary CD25/*ortho*IL-2Rβ/*ortho*IL-2 complex that correlate with their respective potency on *ortho*IL-2Rβ T cells (fig. S1).

In clinical ACT regimens, patient-derived T cells for ACT are expanded in IL-2 before re-infusion in order to obtain sufficient numbers of therapeutic cells with the desired genotype/phenotype (2). We explored the in vitro activity of *ortho*IL-2 on activated primary mouse CD8$^+$ T cells engineered to express the *ortho*IL-2Rβ and a yellow fluorescent protein (YFP) to distinguish modified (YFP$^+$) and unmodified (YFP$^-$) cells (Fig. 2A). The transcription factor STAT5 is phosphorylated upon IL-2 engagement with the IL-2R and translocates to the nucleus, where it promotes the proliferation and cell cycle progression of T cells (11). Wild-type IL-2 induced the phosphorylation of STAT5 (pSTAT5) in both wild-type and *ortho*IL-2Rβ CD8$^+$ T cells with similar potency and signaling amplitude, indicating functional signal transduction through the wild-type receptor but not *ortho*IL-2Rβ (Fig. 2B). By comparison, *ortho*IL-2 1G12 potently activated STAT5 on *ortho*IL-2Rβ–transduced T cells, with a potency increase by a factor of ~5 relative to wild-type T cells. *Ortho*IL-2 3A10 induced somewhat weaker, albeit selective pSTAT5 on *ortho*IL-2Rβ–expressing but not wild-type T cells (Fig. 2, B, D, and E). These results were consistent with the biased binding of the *ortho*IL-2s to the *ortho*IL-2Rβ, which translated into the selective or specific expansion of *ortho*IL-2Rβ T cells cultured ex vivo in *ortho*IL-2 1G12 or 3A10, respectively (Fig. 2, C and D). The *ortho*IL-2Rβ–transduced T cells cultured in saturating concentrations of *ortho*IL-2 3A10 became enriched to near homogeneity after 3 to 5 days (Fig. 2F).

IL-2 is indispensable for the development and function of regulatory T cells (T$_{regs}$) (12), which are sensitive to IL-2 as a result of constitutive expression of CD25 and require IL-2Rβ–dependent activation of STAT5 signaling for survival and function (13). Both *ortho*IL-2 1G12 and 3A10 retained specificity for T$_{regs}$ modified to express the *ortho*IL-2Rβ, with potency similar to that on CD8$^+$ T cells (Fig. 2G and fig. S9, A and B). In addition to cells that naturally respond to IL-2, activation of *ortho*IL-2Rβ signaling pathways with *ortho*IL-2 could, in principle, be achieved in any cell type that also expresses the IL-2Rγ. Activated mouse B cells expressed the IL-2Rγ but lacked appreciable levels of IL-2Rβ (14, 15) and were relatively insensitive to IL-2–dependent STAT5 activation (Fig. 2H and fig. S9, E and F). Transduction of the *ortho*IL-Rβ into activated B cells rendered them responsive to *ortho*IL-2 (Fig. 2H and fig. S9, E and F), but with reduced potency and increased specificity relative to T cells. Specificity was due to the lack of appreciable wild-type IL-2Rβ on B cells (fig. S9E).

In a host with an intact immune system, adoptively transferred T cells must compete with host cells for survival signals such as IL-2 (16). However, unlike wild-type IL-2, there should be minimal competition from endogenous cells for *ortho*IL-2 consumption. Thus, we determined the in vivo activity of *ortho*IL-2 and *ortho*IL-2Rβ T cells in mice with intact immune systems. A mixture of wild-type and *ortho*IL-2Rβ CD8$^+$ T cells was adoptively

transferred into wild-type mice, and the impact of IL-2 and *ortho*IL-2 administration on transplanted T cells and the host immune system was quantified (Fig. 3A). *Ortho*IL-2 1G12 significantly expanded CD8$^+$ T cells transduced with the *ortho*IL-2Rβ at doses equivalent to or lower than wild-type IL-2, which acted through the endogenous IL-2Rβ expressed in both wild-type and *ortho*IL-2Rβ T cells (Fig. 3B and fig. S10). The selectivity of *ortho*IL-2 1G12 for *ortho*IL-2Rβ T cells was dose-dependent, with increased activity on wild-type cells at increased dose amounts and/or frequency of treatment (Fig. 3, B and C, and figs. S10 to S12). These results were consistent with the in vitro selectivity of *ortho*IL-2 1G12, although it remained possible that *ortho*IL-2 1G12 signaling through the *ortho*IL-2Rβ could trigger endogenous IL-2 production by the *ortho*IL-2Rβ T cells, leading to indirect signaling through the wild-type IL-2R in cis or trans.

At high doses and twice-daily administration, *ortho*IL-2 3A10 resulted in the substantial expansion of *ortho*IL-2Rβ T cells with high specificity and no wild-type T cell expansion (Fig. 3, B and C, and figs. S11 and S12). This finding suggests that the effects of high-dose *ortho*IL-2 1G12 treatment were due not to induction of endogenous IL-2 by *ortho*IL-2Rβ CD8$^+$ T cells, but rather to low-level cross-reactivity with the wild-type IL-2Rβ by this molecule. The *ortho*IL-2 variants also promoted the in vivo expansion of *ortho*IL-2Rβ CD4$^+$ effector T cell (T$_{eff}$) (Fig. 3I and fig. S12) and *ortho*IL-2Rβ CD4$^+$ T$_{reg}$ (fig. S9, C and D) cell subsets with specificity similar to that in CD8$^+$ T cells.

The two different *ortho*IL-2 variants exhibited specificities in vivo that mirrored their relative specificities in vitro. Despite its ability to activate wild-type IL-2Rβ signaling, albeit with about one order of magnitude less potency than *ortho*IL-2Rβ signaling, *ortho*IL-2 1G12 administration was relatively specific for *ortho*IL-2Rβ T cells in vivo (Fig. 3, B to H, and figs. S10 to S12). In mice treated twice daily with *ortho*IL-2 1G12 only, CD4$^+$ T$_{regs}$ were elevated to a substantially lower degree than observed in IL-2–treated mice (Fig. 3F). However, the *ortho*IL-2 3A10 variant, consistent with the lack of wild-type IL-2Rβ signaling, had no detectable activity on host cell subset numbers (fig. S11) or expression of CD25, PD-1, and TIM-3, which are up-regulated by early or late IL-2R signaling (fig. S13).

To improve in vivo half-life and enable more convenient dosing, we fused IL-2 and *ortho*IL-2 to mouse serum albumin (17) (MSA), which has been shown to extend the half-life of mouse IL-2 from 5 hours to 50 hours (18). Fusion to MSA had little to no impact on IL-2– or *ortho*IL-2–dependent T cell proliferation in vitro (fig. S14); however, the in vivo activity was greatly enhanced. Fusion of *ortho*IL-2 1G12 to MSA substantially increased its activity on cells that express the wild-type IL-2R relative to native *ortho*IL-2 1G12, leading to increased off-target effects and toxicity (fig. S15). However, the MSA–*ortho*IL-2 3A10 fusion protein retained exquisite specificity for *ortho*IL-2Rβ T cells (fig. S16).

One of the major limitations of IL-2 in the clinic is that IL-2 toxicity limits the use of high-dose IL-2 therapy for metastatic cancer and as an adjuvant to adoptive T cell therapy (12). IL-2 administered as a MSA fusion resulted in a number of dose-dependent and dose-accumulating toxicities that led to weight loss, restricted mobility, hypothermia, ruffled fur, hunched posture, splenomegaly, lymphomegaly, and death (Fig. 3, J to L, and figs. S15 to

S18). In contrast, MSA–*ortho*IL-2 3A10 was nontoxic at all doses evaluated. MSA–*ortho*IL-2 3A10 activity was negligible on all IL-2–responsive host cell subsets evaluated.

In addition to its role as a proliferative cytokine, IL-2 is a potent effector cytokine capable of activating cytotoxic T cell functions and T cell inflammatory pathways (19). We determined the capacity of adoptively transferred *ortho*IL-2Rβ CD8+ T cells to produce interferon-γ (IFN-γ) and cell surface levels of the immune inhibitory receptors PD-1 and TIM-3 after expansion in vivo with *ortho*IL-2. TIM-3 expression correlates with a highly dysfunctional CD8+ T cell state, whereas PD-1 expression is associated with both T cell activation and exhaustion (20). *Ortho*IL-2Rβ T cells expanded in *ortho*IL-2 produced significantly more IFN-γ than IL-2–expanded cells (Fig. 4A). PD-1 levels were similar on *ortho*IL-2Rβ T cells from both IL-2– and *ortho*IL-2–treated mice (Fig. 4B). Interestingly, TIM-3 levels were significantly lower on *ortho*IL-2Rβ T cells from mice treated with *ortho*IL-2 relative to those treated with IL-2 (Fig. 4B).

The differential activity of *ortho*IL-2 on both T cell expansion and function may be due to increased bioavailability of *ortho*IL-2 for *ortho*IL-2Rβ T cells as the result of a reduced antigen sink or alternative host factors influenced by IL-2 but not *ortho*IL-2, which in turn may influence the function of transplanted T cells. For instance, IL-2 but not *ortho*IL-2 treatment increased host CD4+ and CD8+ T cell IFN-γ production upon ex vivo restimulation (Fig. 3, M to O) and increased the serum concentration of numerous inflammatory cytokines, including IFN-γ, IL-4, IL-5, IL-6, and IL-13 (Fig. 3, P and Q, and fig. S17). The ability to decouple direct IL-2 activity on transplanted T cells from indirect host bystander effects using *ortho*IL-2/IL-2R pairs may have important therapeutic implications.

To investigate prospective clinical applications of orthogonal IL-2/IL-2R pairs, we determined the efficacy of tumor-specific *ortho*IL-2Rβ T cells in the B16-F10 mouse model of melanoma. Transgenic pmel-1 T cell receptor (TCR) cells (pmel-1 T cells) express a high-affinity TCR that recognizes the B16-F10 specific ortholog of human gp100 (19), a self antigen overexpressed in human melanoma (Fig. 4, C and D). Adoptive transfer of pmel-1 T cells in combination with lymphocyte depletion and IL-2 administration can model ACT approaches to treat human cancer. Adoptive transfer of pmel-1 T cells accompanied by five daily injections of IL-2 significantly delayed tumor growth in mice and increased survival relative to mice treated only with T cells and saline (Fig. 4, E to G). Transfer of *ortho*IL-2Rβ pmel-1 T cells followed by treatment with native *ortho*IL-2 1G12 at a dose that had minimal activity on wild-type IL-2R cells (fig. S10) produced a significant tumor growth delay and survival advantage that mirrored the IL-2 treatment group (Fig. 4, E and F). Similar antitumor responses were observed in mice treated with *ortho*IL-2Rβ pmel-1 T cells and MSA–*ortho*IL-2 3A10 (Fig. 4, G and H). There was no therapeutic benefit of *ortho*IL-2 in mice that received wild-type pmel-1 T cells, indicating that *ortho*IL-2 activity is dependent on expression of the *ortho*IL-2Rβ in pmel-1 T cells.

Our results constitute an approach to redirect the specificity of IL-2 toward engineered T cells using orthogonal IL-2 cytokine-receptor pairs, which enables the selective expansion of desired T cell subsets in settings of adoptive cell therapy, but with limited off-target activity

and negligible toxicity. Engineering orthogonal molecular recognition at a protein–small molecule or protein-protein interface has resulted in synthetic enzymes, kinases, transcription factors, and receptors with controllable biological functions, but here we apply this concept to protein interactions with cell surface receptors to control signaling specificity and downstream cellular functions (21–28). Orthogonal IL-2/IL-2R pairs may be useful not only as a research tool but in the clinic to specifically enrich transduced T cells that express a target gene of interest, such as a CAR or engineered TCR, when coupled with expression of the *ortho*IL-2Rβ. Our approach, and variations of this orthogonalization strategy, may be applicable to other cytokines, growth factors, hormones, and ligand-receptor interactions to decipher and manipulate otherwise complex biological systems.

Supplementary Material

Refer to Web version on PubMed Central for supplementary material.

Acknowledgments

REFERENCES AND NOTES

1. Kalos M, June CH. Immunity. 2013; 39:49–60. [PubMed: 23890063]

2. Rosenberg SA, Restifo NP. Science. 2015; 348:62–68. [PubMed: 25838374]

3. Yee C, et al. Proc Natl Acad Sci USA. 2002; 99:16168–16173. [PubMed: 12427970]

4. Andersen R, et al. Clin Cancer Res. 2016; 22:3734–3745. [PubMed: 27006492]

5. Rosenberg SA. J Immunol. 2014; 192:5451–5458. [PubMed: 24907378]

6. Wang X, Rickert M, Garcia KC. Science. 2005; 310:1159–1163. [PubMed: 16293754]

7. Levin AM, et al. Nature. 2012; 484:529–533. [PubMed: 22446627]

8. Shanafelt AB, et al. Nat Biotechnol. 2000; 18:1197–1202. [PubMed: 11062441]

9. Rickert M, Boulanger MJ, Goriatcheva N, Garcia KC. J Mol Biol. 2004; 339:1115–1128. [PubMed: 15178252]

10. Roessler E, et al. Proc Natl Acad Sci USA. 1994; 91:3344–3347. [PubMed: 8159750]

11. Moriggl R, et al. Immunity. 1999; 10:249–259. [PubMed: 10072077]

12. Malek TR. Annu Rev Immunol. 2008; 26:453–479. [PubMed: 18062768]

13. Klatzmann D, Abbas AK. Nat Rev Immunol. 2015; 15:283–294. [PubMed: 25882245]

14. Amu S, Gjertsson I, Tarkowski A, Brisslert M. Scand J Immunol. 2006; 64:482–492. [PubMed: 17032240]

15. Boyman O, Sprent J. Nat Rev Immunol. 2012; 12:180–190. [PubMed: 22343569]

16. Gattinoni L, et al. J Exp Med. 2005; 202:907–912. [PubMed: 16203864]

17. Sockolosky JT, Szoka FC. Adv Drug Deliv Rev. 2015; 91:109–124. [PubMed: 25703189]

18. Zhu EFF, et al. Cancer Cell. 2015; 27:489–501. [PubMed: 25873172]

19. Overwijk WW, et al. J Exp Med. 2003; 198:569–580. [PubMed: 12925674]

20. Sakuishi K, et al. J Exp Med. 2010; 207:2187–2194. [PubMed: 20819927]

21. Baud MGJ, et al. Science. 2014; 346:638–641. [PubMed: 25323695]

22. Atwell S, Ultsch M, De Vos AM, Wells JA. Science. 1997; 278:1125–1128. [PubMed: 9353194]

23. Spencer DM, Wandless TJ, Schreiber SL, Crabtree GR. Science. 1993; 262:1019–1024. [PubMed: 7694365]

24. Mandell DJ, Kortemme T. Nat Chem Biol. 2009; 5:797–807. [PubMed: 19841629]

25. Kapp GT, et al. Proc Natl Acad Sci USA. 2012; 109:5277–5282. [PubMed: 22403064]

26. Park JS, et al. Proc Natl Acad Sci USA. 2014; 111:5896–5901. [PubMed: 24711398]

27. Lewis SM, et al. Nat Biotechnol. 2014; 32:191–198. [PubMed: 24463572]

28. Wu CY, Roybal KT, Puchner EM, Onuffer J, Lim WA. Science. 2015; 350:aab4077. [PubMed: 26405231]

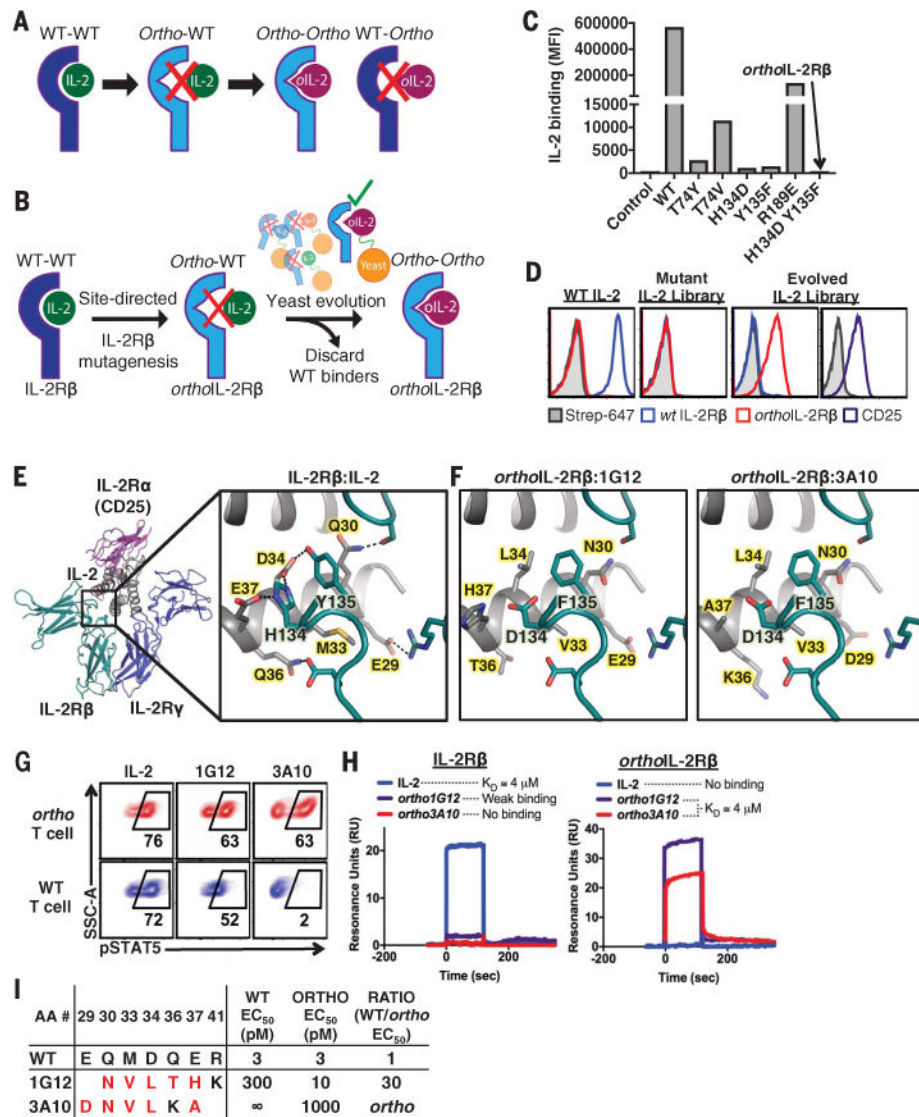**Fig. 1. Engineering and characterization of orthogonal IL-2 and IL-2R pairs**

(**A**) Schematic overview of orthogonal IL-2/IL-2R pairs, consisting of a mutant IL-2 cytokine and mutant IL-2R that interact specifically with each other but do not cross-react with their wild-type counterparts. (**B**) Strategy used to engineer orthogonal IL-2/IL-2Rβ pairs. (**C**) Wild-type and mutant IL-2Rβ tetramer binding to wild-type IL-2 displayed on yeast by fluorescence-activated cell sorting. MFI, mean fluorescence intensity. Data are representative of two independent experiments. (**D**) Histograms of wild-type IL-2Rβ (blue), *ortho*IL-2Rβ (red), or CD25 (purple) binding to yeast-displayed wild-type IL-2, the naïve mutant IL-2 yeast library, or mutant IL-2 yeast clones after in vitro evolution. In vitro evolution of three independent mutant IL-2 yeast libraries (fig. S4) yielded similar results. (**E**) Homology model of the mouse IL-2/IL-2Rβ structure and the site I interface of IL-2 (gray) and contacts with IL-2Rβ His[134] and Tyr[135] (teal). Dashed lines indicate potential polar contacts. (**F**) Model of the *ortho*IL-2/*ortho*IL-2Rβ interactions. (**G**) Off-yeast pSTAT5 functional screen of IL-2 mutant activity on wild-type and *ortho*IL-2Rβ CTLL-2 T cells. (**H**)

Representative surface plasmon resonance (SPR) sensograms of wild-type and *ortho*IL-2 binding to wild-type IL-2Rβ or *ortho*IL-2Rβ. Data are representative of two independent experiments. K_D, dissociation constant. (**I**) Sequences of wild-type (WT) IL-2, *ortho*IL-2 1G12, and *ortho*IL-2 3A10 and corresponding in vitro bioactivity (pSTAT5 EC_{50}) on wild-type and *ortho*IL-2Rβ CTLL-2 Tcells. Amino acid codes: A, Ala; D, Asp; E, Glu; F, Phe; H, His; K, Lys; L, Leu; M, Met; N, Asn; Q, Gln; T, Thr; V, Val; Y, Tyr.
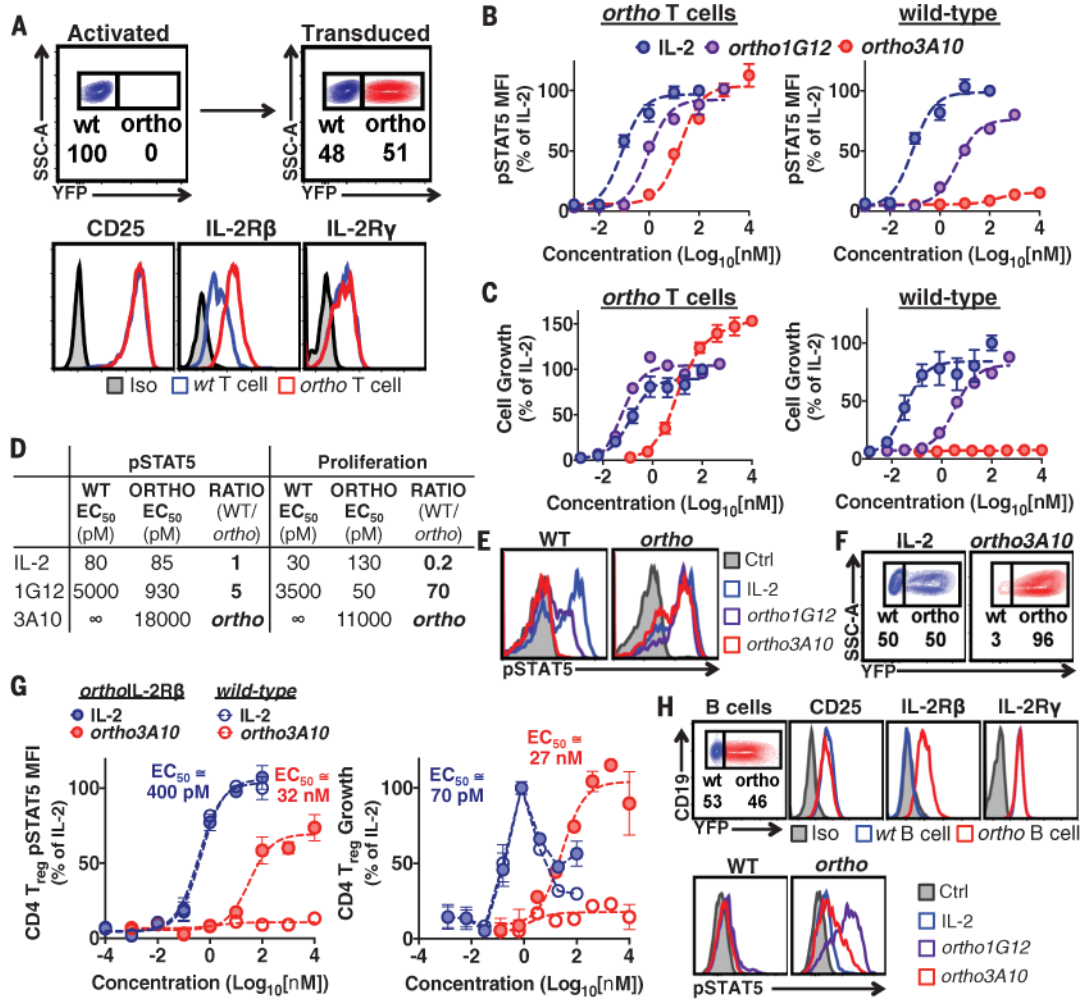
Fig. 2. *Ortho*IL-2 signals through the *ortho*IL-2R expressed in primary mouse lymphocyte subsets, resulting in specific expansion of CD4 and CD8 T cells in vitro

(**A**) Flow cytometry data of mouse T cells transduced with the *ortho*IL-2Rβ and a YFP reporter (top panels) and associated cell surface levels of CD25, IL-2Rβ, and IL-2Rγ. (**B** to **F**) Dose-response curves of (B) STAT5 phosphorylation after 20 min of stimulation and (C) proliferation of wild-type (open circles) and *ortho*IL-2Rβ (solid circles) CD8$^+$ Tcells cultured for 4 days in IL-2 or *ortho*IL-2; (D) table of respective pSTAT5 and proliferation EC$_{50}$ from data in (B) and (C). Representative histograms of (E) STAT5 phosphorylation and (F) scatterplots of CD8$^+$ wild-type (YFP$^-$) and *ortho*IL-2Rβ (YFP$^+$) T cells expanded in IL-2. Data are means ± SD ($n = 3$ biological replicates). Dashed lines represent curves fit to a log (agonist) versus response (three parameters) model in Prism. (**G**) Dose-response curves of STAT5 phosphorylation (left) and proliferation (right) of wild-type and *ortho*IL-2Rβ CD4$^+$ T$_{regs}$ cultured in IL-2 or *ortho*IL-2. Data are means ± SD ($n = 3$ biological replicates). (**H**) Representative histograms of primary mouse B cells transduced with the *ortho*IL-2Rβ and stimulated with the indicated cytokines for quantification of intracellular pSTAT5 as in fig. S9.
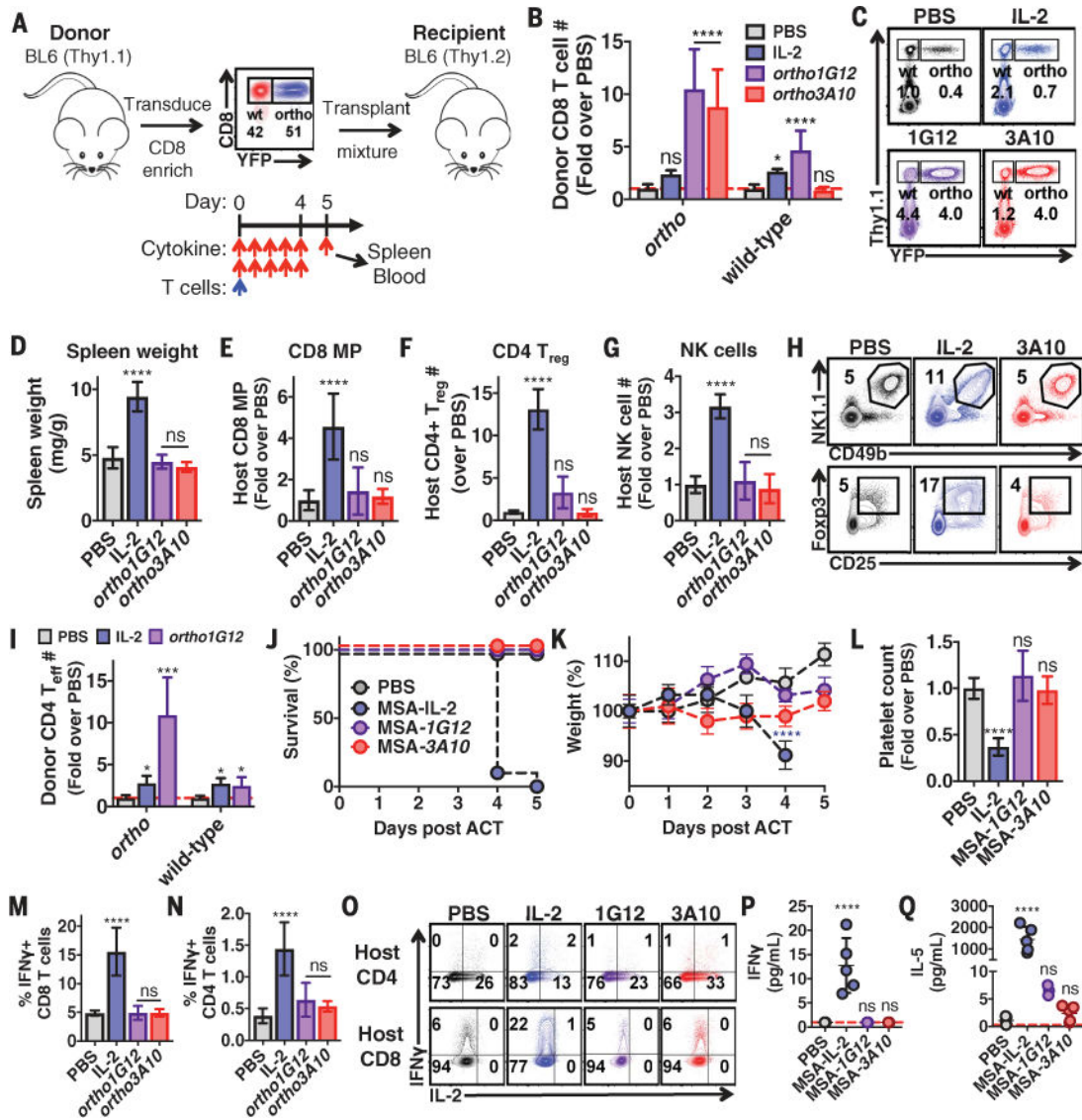
Fig. 3. *Ortho*IL-2 promotes the specific expansion of *ortho*IL-2Rβ–modified T cells in mice with negligible toxicity

(**A**) Schematic of the adoptive CD8+ T cell transplant mouse model. (**B**) Quantification of donor wild-type and *ortho* CD8+ T cells in the spleen of recipient mice treated twice daily with phosphate-buffered saline (PBS), IL-2 (250,000 IU/dose), *ortho*IL-2 1G12 (250,000 IU/dose), or *ortho*IL-2 3A10 (2,500,000 IU/dose). (**C**) Representative flow cytometry data quantified in (B) depicting donor (Thy1.1+) wild-type (YFP−) and *ortho*IL-2Rβ (YFP+) CD8+ T cells in the spleen of recipient mice. (**D**) Spleen weight of mice treated in (B) normalized to total body weight on day of killing. (**E** to **G**) Quantification of exogenous cytokine administration on host (E) CD8+ memory phenotype T cell (MP, CD44+CD62L+), (F) CD4+ T_{reg} (CD25+Foxp3+), and (G) natural killer (NK) cell (CD3-NK1.1+CD49b+) numbers in the spleen of mice treated in (A). (**H**) Representative flow cytometry data as quantified in (F) and (G). Data in (B) to (H) are means ± SD (*n* = 5 mice per group). *$P <$ 0.05, ****$P <$ 0.0001 [analysis of variance (ANOVA)]; ns, not significant. (**I**) Quantification

of donor wild-type and *ortho*IL-2Rβ CD4$^+$ T$_{eff}$ in the spleen of recipient mice treated once daily with PBS, IL-2 (250,000 IU/dose), or *ortho*IL-2 1G12 (1,000,000 IU/dose). Data are means ± SD and are representative of two independent experiments ($n = 4$ mice per group). *$P < 0.05$, ***$P < 0.001$ (ANOVA). (**J**) Survival of mice that received a mixture of wild-type and *ortho*IL-2Rβ CD8$^+$ T cells followed by daily administration of IL-2 or *ortho*IL-2 fused to MSA. All mice received a total of 250,000 IU/day of the respective MSA fusion protein on an IL-2 basis for 5 days. (**K**) Mouse body weight over time normalized to the group average on day 0 as treated in (J). (**L**) Platelet counts in peripheral blood on day 4 as treated in (J). Data in (J) to (L) are means ± SD ($n = 5$ mice per group). ****$P < 0.0001$ (ANOVA). (**M** to **O**) Quantification of cytokine administration on host (M) CD8$^+$ and (N) CD4$^+$ T cell production of IFN-γ upon ex vivo restimulation with phorbol 12-myristate 13-acetate (PMA) and ionomycin. (O) Representative flow cytometry data as quantified in (M) and (N). (**P** and **Q**) Serum (P) IFN-γ and (Q) IL-5 concentrations on day 7 in mice treated daily with PBS or with MSA–IL-2, MSA-1G12, or MSA-3A10 (each 25,000 IU/dose) for 7 days. Data are means ± SD ($n = 5$ mice per group). ****$P < 0.0001$ (ANOVA).
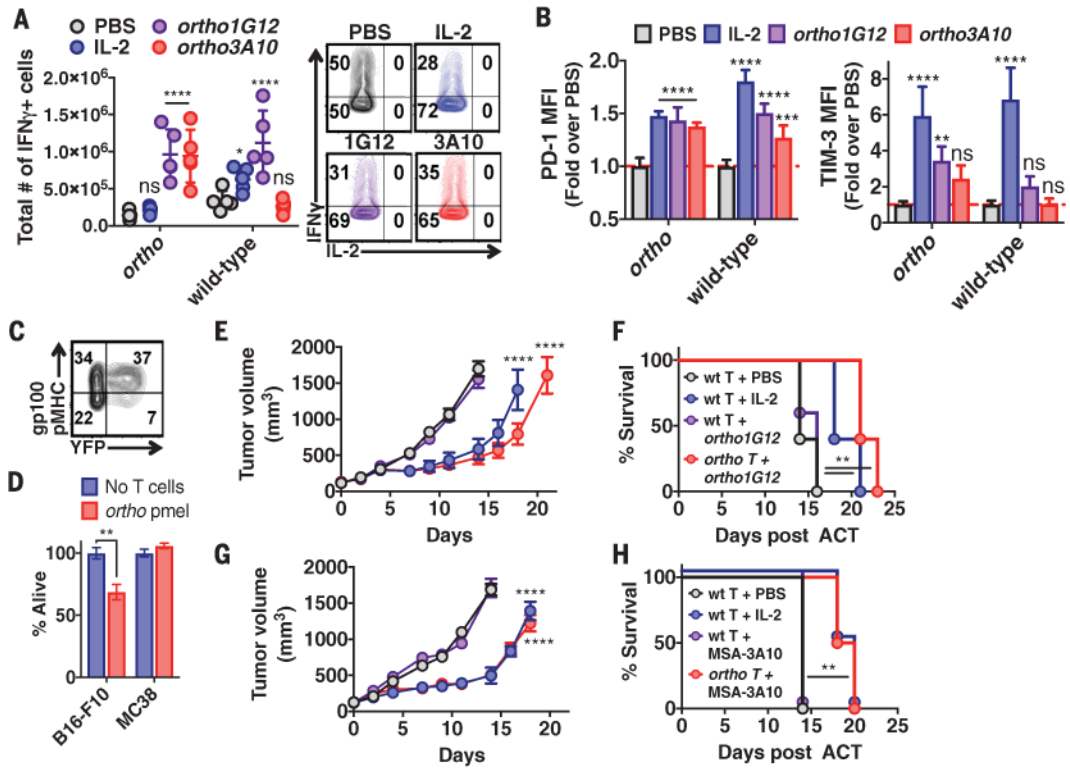
Fig. 4. *Ortho*IL-2–expanded T cells retain effector function and promote an antitumor response against syngeneic B16-F10 tumors in mice

(**A**) Quantification of total number of IFN-γ–positive wild-type or *ortho*IL-2Rβ CD8+ T cells recovered from the spleen as treated in Fig. 3 (left) and representative flow cytometry data (right). (**B**) Cell surface expression levels of PD-1 (left) and TIM-3 (right) on wild-type and *ortho*IL-2Rβ CD8+ T cells in the spleen after administration of the indicated cytokines. Data are means ± SD ($n = 5$ mice per group). *$P < 0.05$, ****$P < 0.0001$ (ANOVA). (**C**) gp100 pMHC tetramer staining of *ortho*IL-2Rβ–transduced pmel-1 transgenic CD8+ T cells. (**D**) In vitro cytotoxicity of *ortho*IL-2Rβ pmel-1 transgenic T cells against antigen-positive (B16-F10) but not antigen-negative (MC38) tumor cells at a 20:1 (E:T) ratio. Data are means ± SD ($n = 3$ biological replicates). **$P < 0.01$ (Student t test). (**E** and **F**) Tumor growth (E) and survival (F) of C57BL/6J mice bearing subcutaneous B16-F10 tumors treated with wild-type (wt T) or *ortho*IL-2Rβ pmel-1 transgenic CD8+ T cells (*ortho* T) and IL-2 or *ortho*IL-2 1G12. Data are means ± SEM ($n = 5$ mice per group). ****$P < 0.0001$ (two-way ANOVA) (E); **$P < 0.01$ (log-rank test) (F). (**G** and **H**) Tumor growth (G) and survival (H) of C57BL/6J mice bearing subcutaneous B16-F10 tumors treated with wild-type (wt T) or *ortho*IL-2Rβ pmel-1 transgenic CD8+ T cells (*ortho* T) and IL-2 or *ortho*IL-2 3A10 fused to MSA. Data are means ± SEM ($n = 4$ mice per group). ****$P < 0.0001$ (two-way ANOVA) (G); **$P < 0.01$ (log-rank test) (H).